A Divot in the Size Distribution of the Kuiper Belt's Scattering Objects

C. Shankman, B. J. Gladman,

Department of Physics and Astronomy, The University of British Columbia, 6224 Agriculture Road, Vancouver, BC, V6T 1Z1

N. Kaib

Department of Physics and Astronomy, Queens University, Canada

J.J. Kavelaars

Herzberg Institute of Astrophysics, National Research Council of Canada, Victoria, BC, Canada

and

J.M. Petit

Institut UTINAM, CNRS-Université de Franche-Comté, Besançon, France

Received _____; accepted _____

ABSTRACT

Via joint analysis of a calibrated telescopic survey, which found scattering Kuiper Belt objects, and models of their expected orbital distribution, we measure the form of the scattering object's size distribution. Ruling out a single power-law at greater than 99% confidence, we constrain the form of the size distribution and find that, surprisingly, our analysis favours a very sudden decrease (a divot) in the number distribution as diameters decrease below 100 km, with the number of smaller objects then rising again as expected via collisional equilibrium. Extrapolating at this collisional equilibrium slope produced enough kilometer-scale scattering objects to supply the nearby Jupiter-Family comets. Our interpretation is that this divot feature is a preserved relic of the size distribution made by planetesimal formation, now "frozen in" to portions of the Kuiper Belt sharing a "hot" orbital inclination distribution, explaining several puzzles in Kuiper Belt science. Additionally, we show that to match today's scattering-object inclination distribution, the supply source that was scattered outward must have already been vertically heated to of order 10°.

Subject headings: comets: general — Kuiper belt: general

1. Introduction

Measurements of the Kuiper Belt's size distribution (number at each diameter D) constrain accretional processes at planet formation and, potentially, subsequent collisional or physical evolution. Because astronomers observe brightnesses rather than D, object absolute magnitudes H are tabulated as the observable proxy for the size distribution. If the albedo p is known, H is convertible to D; for 5% albedo a $D = 100$-km object has H=9.16 in g band. Using H_g magnitudes avoids uncertainties introduced by assuming the unknown albedos.

Collisional and accretional theories suggest exponential forms for the $N(H)$ distribution. A differential number distribution of the form $\mathrm{d}N/\mathrm{d}H \propto 10^{\alpha H_g}$ with a logarithmic 'slope' α corresponds to a power-law D distribution $\mathrm{d}N/\mathrm{d}D \propto D^{-(5\alpha+1)}$. Although power-law D distributions provide acceptable fits to Kuiper Belt surveys over spans of a few magnitudes in H, departures from single power laws are necessary over larger H ranges (Jewitt et al. 1988; Gladman et al. 2001; Bernstein et al. 2004; Fuentes & Holman 2008; Fraser & Kavelaars 2008). For the steep (α=0.8–1.2) distributions seen in the Kuiper Belt, detections are dominated by objects near the largest H magnitude (smallest size) visible in a given survey. An $\alpha > 0.6$ slope cannot continue as $H \to \infty$ ($D \to 0$ km) or the total mass diverges; thus a slope change (generically called a break) is required. Evidence of such a break now exists for trans-Neptunian objects (TNOs) in the main Kuiper Belt (at distances $d \simeq$ 38–46 AU), both near the sensitivity limit of ground-based telescopic surveys (Fraser & Kavelaars 2008; Fuentes & Holman 2008) (reaching $H_g \sim$9–10 at 40 AU) and from deeper HST (Bernstein et al. 2004) observations ($H_g \sim$13 at 40 AU). This break has been modelled as a gradual transition to a smaller value of α, a "knee".

Probing beyond a break is difficult because small TNOs are faint. This problem is reduced when observing the scattering objects (SOs); these are mostly TNOs with perihelia

$q \leq 35$ AU (see below) and thus smaller objects are detectable as they come near the observer. At any time some SOs are only $d = 20$–30 AU away, allowing a 4-m telescope, in excellent conditions, to detect objects down to $H_g \sim 12$. For a monotonically increasing number distribution $N(H_g)$, the abundant small objects at the observable volume's innermost edge should dominate the detected sample. This is not what our survey found, necessitating a relative lack of small SOs.

2. Models

Several models of the SO orbital element distribution were exposed to the calibrated observational biases of the Canada France Ecliptic Plane Survey (CFEPS) in order to quantitatively constrain the intrinsic $N(H_g)$ distribution. Drawing SOs from an orbital distribution model, and selecting H_g from a candidate $N(H_g)$ distribution, the CFEPS survey simulator (Jones et al. 2006) determines each object's observability and produces a set of "simulated detections" expected from the model.

Two different simulations of this population are from a modified version of Kaib et al. (2011b) (henceforth KRQ11). KRQ11 focuses on the effects of solar migration in the Milky Way on Oort Cloud structure. While this is not the focus of the current work, we can use the KRQ11 control simulations, which assume an unchanging local galactic environment like our current one.

To test the sensitivity of our results to the choice of the dynamical context, we performed the same analysis on an independent model. Gladman & Chan (2006) modelled the scattering of objects an initial Solar System with an additional planet (of order Earth's size). As previously reported (Petit et al. 2011) this model also (perhaps surprisingly) reasonably represents the current SO (a, q) distribution , although too "cold" in inclinations.

In fact, this model and the cold KRQ11 model produced very similar results. We find that the results for this model are nearly identical to KRQ11 results, showing that our conclusions are not strongly dependent on the model of Solar System history, as the objects that are currently in the Centaur and detectable SO region (mostly a <200 AU) today have, unsurprisingly, almost forgotten their initial state except for the the inclination distribution. Thus, the current SO orbital distribution is not diagnostic of the number and position of the planets early in the Solar System's history.

3. Observations

CFEPS provided a set of detections of outer Solar System objects in a precisely calibrated survey (Jones et al. 2006; Kavelaars et al. 2009) whose pointing history, detection efficiency, and tracking performance were recorded. The final set of TNO detections (with full high-precision orbits) and the fully calibrated pointing history make up the L7 release (Petit et al. 2011). This absolute calibration of CFEPS allows a model of the present orbital (and size) distribution of to be passed through the CFEPS Survey Simulator, yielding a set of simulated detections whose orbital and H_g distributions can be compared to the real detections.

Our models provide orbital distributions of all TNOs. The "scattering" TNOs are then selected out of the final 10 Myr stage of the model integrations using the criteria: variation of a >1.5 AU in semimajor axis during 10 Myr, with $a < 1000$ AU (Gladman et al. 2008; Morbidelli et al. 2004). Historically, a simple q cut was used to isolate the "scattered disk" (Duncan & Levison 1997; Luu et al. 1997; Trujillo et al. 2000), which undesirably includes resonant objects and most inner main-belt TNOs.

The CFEPS SO sample consists of 9 detected objects (Table 1). In addition, we

include two objects discovered in a high-latitude extension survey (covering $\simeq$ 470 sqdg in 2007–2008, extending up to 65° ecliptic latitude), which was fully calibrated in the same way as CFEPS.

The CFEPS Survey Simulator was used to observationally bias the three models. Given an orbital model and a candidate $N(H_g)$, the simulator determines if one of the survey fields would have detected test model objects, producing a distribution of "detected" objects as if the model were the true orbital distribution. The resulting set of "observationally-biased" objects are statistically compared to the set of real detections.

To characterize the form of the $N(H_g)$, we introduce a novel parameterisation which allows for the exploration of distributions with knees and divots (a sudden drop in the differential number of objects followed by a recovery). We parameterised the size distribution (Fig. 2A) with the fixed slope $\alpha_b = 0.8$ (see below) for SOs brighter than a break at $H_g = 9$ ($D \simeq$100 km), allowed an adjustable slope α_f for fainter objects, and an adjustable contrast $c \geq 1$.

The H_g-magnitudes are drawn from one of three types of distributions:

1. a single exponential of logarithmic slope α, **2.** a $N(H_g)$ with a knee (contrast c =1). That is, one slope α_b for SOs with $H_g < H_{knee}$ and α_f for $H_g > H_{knee}$, where the $N(H_g)$ distribution is continuous across the knee at H_{knee} and negative slopes α_f are allowed as per suggestions in the literature (Bernstein et al. 2004), and **3.** one slope α_b to a divot at H_{divot}, which is a sudden drop in differential number by a factor c, with a potentially different slope α_f beyond the cliff at $H = H_{divot}$. Although in reality the discontinuity is unlikely to be an instantaneous drop, our data do not merit trying to constrain the values of the expected steep negative slope and small extent over which it drops; collisional models (Fraser 2009; Campo Bagatin & Benavidez 2012) do show collisional divots where the drop occurs over short diameter range of much less than a factor of two in D (a few tenths of

magnitude in H_g).

In principle there are four parameters: α_b, α_f, H_{divot}, and c (Fig. 2). For $H_g < 9$ a single power law of $\alpha_b \simeq 0.8$ does match our detections, and we elected to fix this slope at that value with the unifying philosophy that all the hot transneptunian populations share this same hot slope; $\alpha_b = 0.8$ matches both the hot Classical belt, measured down to $H_g \simeq 8.0$ (Petit et al. 2011; Fraser & Kavelaars 2008; Fuentes & Holman 2008), and to the 3:2 resonators, measured down to $H_g \simeq 9.0$ (Gladman et al. 2012), both of which appear consistent with single power laws for H brighter than those limits. Our detections require a transition around H_g =9–10 to explain the lack of small detections; we thus fix the knee/divot for our analysis at $H_g = 9$ (slightly larger than D=100 km for 5% g-band albedo). This leaves only two free parameters: the contrast c at the divot and the slope α_f for objects with absolute magnitudes fainter than the divot/knee.

To assess a match, the Anderson-Darling (AD) statistic is calculated between our 11-object sample and the distribution of simulated detections from the model, for each orbital parameter. An AD significance level of $< 5\%$ means a rejection of the hypothesis that the real SO observations could be drawn from the simulated detections at the 95% confidence level (for that orbital parameter). For a model to not be rejectable we use the criteria that none of the q, d, i, and H_g distributions can be rejectable at $> 95\%$ confidence.

4. Absolute Magnitude Distribution

The observational bias is strong (Fig. 1) , but when accurately calibrated allows us to constrain the H_g distribution's form. Single power-laws predict significantly more close-in detections than were seen by CFEPS; for a slope of $\alpha = 0.8$, roughly half of the expected detections (Fig. 1 D's blue dashed curve) should have a distance at detection $d < 23$ AU,

which is the closest real SO in our sample. This observationally biased model predicts that the majority of detected SOs would have orbits with q <20 AU at d = 20–25 AU and be small ($H_g > 9$ or $D \leq 100$ km) objects, in contrast to our detections, which demonstrates that our observations are sensitive beyond the break. This discrepancy exists for all of our models when using a single power-law, and thus must arise from the assumed $N(H_g)$. We rule out a single power-law at 95% confidence.

Our relatively small sample is powerful because our detected SOs span the break, and when coupled with the precise CFEPS calibration, allows the non-detection of H_g =10-12 SOs (several magnitudes past the divot) to provide a strong constraint on $N(H_g)$. CFEPS detected moving objects as close as 20 AU with no rate of motion dependence down to this limit. Because our orbits are accurate, we can separate the SOs from the other hot populations, and use a dynamical model specific to the SOs.

In Fig. 1, our best $N(H_g)$ case has the obvious and previously-known problem that the model's orbital inclinations are mostly lower than the true population's (Petit et al. 2011; Gladman et al. 2012). Fig. 1 shows a divot ($c \simeq 6$, $\alpha_f = 0.5$) which produces a good match between the model's expected detections (green curve) and the real SO sample (red), excepting the i problem. Models (Levison et al. 2008) which scatter out a cold TNO population, from $d < 30$ AU and with initial inclination distribution widths $\sigma_i \leq 6^\circ$, to eventually form today's hot population produce current TNO populations where too many low-i detections are expected in observational surveys (Fig. 1B). This is part of growing evidence that the original planetesimal disk supplying today's high-i objects must have already been vertically excited before being scattered out, (Petit et al. 2011; Gladman et al. 2012; Brasser & Morbidelli 2012) which has strong cosmogonic implications for an extended quiescent phase of the early Solar System (Levison et al. 2008). We therefore computed a new SO model with a hotter ($\sigma_i \simeq 12^\circ$) initial disk; this provides an excellent match with

today's SO i-distribution (see Fig. 4) and we constrain $N(H_g)$ below using this model.

To constrain the size distribution, a grid of possible divot contrasts and post-divot slopes was explored. The parameter amongst i, q, d and H which is most rejectable is recorded; Fig. 3 shows acceptability levels for the range of explored parameter pairs (c, α_f). A single power-law of $\alpha = 0.8$ (blue star Fig. 3) has $< 1\%$ probability. We are left with a range of acceptable parameter space, including knee (c=1) and divot (c >1) scenarios; we further constrain $N(H_g)$ by looking to other Kuiper Belt populations.

The so-called hot Kuiper Belt populations (the hot main belt, inner belt, resonant, and detached TNOs) share an i distribution half-width of roughly 15° (Petit et al. 2011) with the SOs, suggesting a cosmogonic link. In analyses of deep luminosity functions dominated by hot main-belt detections, the common conclusion (Bernstein et al. 2004; Fuentes et al. 2010) was that for magnitude $g > 25$ the slope must break to a faint $\alpha_f < 0.3$ value or even become negative in order to explain the lack of detections in the following few magnitudes; beyond this no data exists for the main Kuiper Belt. For SOs and their companion objects (Centaurs), however, many $H_g \gg 9$ objects are known from wide-field surveys, mostly detected at $d < 20$ AU. Thus the SO size distribution cannot remain at $\alpha_f < 0.3$. In fact, measurements of Jupiter Family Comets (JFCs) in the $H_g \approx$14–17 range give slopes $\alpha_f \simeq 0.5 \pm 0.1$ (see Table 6 of Solontoi et al. (2012)). A divot can explain both a relative lack of objects beyond the break and the eventual recovery necessary to provide the JFCs. A divot also motivates the negative slopes measured, as a realistic divot will take the form of a decrease at the break, rather than the sharp discontinuity we use. We prefer the divot solution with α_f =0.5 and $c \simeq$6 (green star Fig. 6) which matches the observations and allows for a single slope $\alpha_f = 0.5$ from the divot out to the H_g >14 Jupiter Family comets whose slope is near the collisional equilibrium value (O'Brien & Greenberg 2005).

5. External Arguments

As the hot populations have similar colours and $D > 100$-km size distributions, it seems likely that they were all transplanted to join a pre-existing cold Kuiper Belt (Petit et al. 2011) during a common event early in the Solar System's history, and would thus logically share the same divot and small D distribution. Such a transplant process has been shown to successfully implant TNOs in the stable Kuiper Belt regions (Levison et al. 2008; Batygin et al. 2011) , although the resonant population ratios and i distribution are problematic (Gladman et al. 2012). We thus look for evidence of such a feature in other hot populations.

5.1. The Neptune Trojans

A survey for Neptune Trojans (Sheppard & Trujillo 2010) provided significant evidence that an $\alpha \sim 0.8$ power law cannot continue for $D < 100$-km Trojans; a divot was not apparent because Trojans significantly smaller were not detected. The dispersed inclination distribution for the Neptune Trojans (Sheppard & Trujillo 2006), although not yet precisely measured, links these objects to all the other resonant populations (Gladman et al. 2012). Sheppard & Trujillo (2010) used Neptune Trojan searches to argue that beyond $m_R \simeq 23$ (corresponding to $H_g \simeq 9$) there was an absence of Trojans due to non-detections, and thus smaller Trojans were missing. Assuming that the Trojans and other resonant TNOs were implanted from a scattering population, and thus share the same size distribution, we confirmed that our divot $N(H_g)$ matches the lack of D <100 km Neptune Torjan detections in the Sheppard & Trujillo (2010) surveys.

Given our analysis, the conclusion would not be that small Neptune Trojans are "missing", but rather that the sudden drop results in the population fainter than the divot

not recovering in on-sky surface density until at least $H_g > 11$, by which point the deepest survey lacked the sensitivity to detect them. If correct, detection of several small ($H_g > 11$) trojans would require surveying $\sim$ 100 square degrees of sky to 26th magnitude at the correct elongation.

5.2. hot Populations

A recent deep telescopic survey (Fraser et al. 2010) estimated $\alpha \simeq 0.40 \pm 0.15$ (within error of our preferred $\alpha_f = 0.5$) from the apparent-magnitude distribution for "close" ($30 < d < 38$) TNOs (orbits were not obtained). These distances are dominated by several hot populations, but the measurement is shallower than the usual hot population slope of 0.8. We calculated H_g magnitudes for the Fraser et al. (2010) sample and find that due to the survey's great depth, this sample is dominated by $H_g > 9$ TNOs and thus appears to measure the post-divot slope.

6. Feasibility of a Divot

A primordial size-distribution wave at small sizes ($D = 2$ km) could propagate (Fraser 2009) to $D \sim$100 km in a dynamically hot ($\Delta v = 2$ km/s) collisional environment after 500 Myr. Alternately, recent modeling of planetesimal creation (Johansen et al. 2007; Morbidelli et al. 2009), suggests that the protosolar nebula may only have produced planetesimals larger than a certain critical diameter, in which case the $\alpha_b = 0.8$ slope and the $D \sim 100$ km divot size are set by planetesimal formation physics; smaller objects appear only later due to collisional fragmentation. These scenarios match our results, where one interprets the hot population's $N(H_g)$ to have been "frozen" when suddenly transplanted (scattered) from a denser region nearer the Sun to the large volume it now

occupies, ending the collisional evolution. An exciting prospect is that the divot directly records a preferential D that planet building produced in the solar-nebula region where the hot TNOs originally formed, and that the divot's depth (which could easily range from c=2–30) measures the integrated collisional evolution (depending on both the duration of the pre-scattering phase and the random speeds present). An initial distribution with no D <100 km TNOs was shown (Campo Bagatin & Benavidez 2012) to evolve into a divot with $c \sim 20$ and $\alpha_f \simeq 0.5$, in the dynamical environment of the Nice model; such a 500-Myr quiescent phase (Gomes et al. 2005) allows a divot to form but the evidence we find for a higher-i early phase may argue instead for a much shorter and more intense collisional environment.

Our divoted $N(H_g)$ produces a cumulative distribution (Fig. 2 B) with a shallow plateau for H_g=9–12, similar to that deduced for the hot population and SOs in deep HST observations (Bernstein et al. 2004; Volk & Malhotra 2008) and estimated for scattering impactors of the saturnian moons (Minton et al. 2012). Our estimate of 2×10^6 SOs with $H_g < 13$ and a slope of $\alpha_f = 0.5$ extrapolates to $\sim 2 \times 10^9$ SOs with H_g <18, providing a sufficient number (Duncan & Levison 1997; Volk & Malhotra 2008) of SOs to feed the Jupiter Family Comets, while satisfying the observed plateau. This novel parameterisation for the $N(H_g)$ distribution (Fig. 2) matches our data set and simultaneously explains the puzzles of the JFC source, along with the "missing" Neptune Trojans, and the known rollover in the Kuiper Belt's luminosity function.

Facilities: CFHT, NRC (HIA)

REFERENCES

Bernstein, G.M. et al. 2004, AJ, 128, 1364

Brasser, R. & Morbidelli, A. 2012 Asteroids, Comets, and Meteors meeting, abstract.

Batygin, K., Brown, M. & Fraser, W. 2011, ApJ, 13, 738

Campo Bagatin & A.,Benavidez, P. 2012, MNRAS, 423, 1254

Duncan, M. & Levison, H.F. 1997, Science, 276, 1670

Elliot, J., Kern, S.D. & Clancy, K.B. 2005, AJ, 129, 1117

Fraser, W. 2009, ApJ, 706, 119

Fraser, W., Brown, M. & Schwamb, M. 2010, Icarus, 210, 944

Fraser, W. & Kavelaars J.J. 2008, Icarus, 198, 452

Fraser, W. & Kavelaars, J.J. 2009, AJ, 137, 72

Fuentes C., & Holman, M. 2008, AJ, 136, 83

Fuentes, C., Holman, M., Trilling, D. & Protopapas, P. 2010, ApJ, 722, 1290

Gladman, B. et al. 2001, AJ, 122, 1051

Gladman, B. & Chan, C. 2006, ApJ, 643, L135

Gladman, B., Kavelaars, J.J., Petit, J.-M., et al. 2009, ApJ, 697, L91

Gladman, B., Lawler, S., Petit, J.-M, et al. 2012, AJ, 144, 23

Gladman, B., Marsden, B.G. & Vanlaerhoven, C. 2008, in The Solar System Beyond Neptune 43

Gomes, R., Levison,H.F., Tsiganis & K., Morbidelli, A. 2005, Nature, 435, 466

Jewitt, D., Luu, J., & Trujillo, C. 1988, AJ115, 2125

Johansen, A., Oishi, J., Mac Low, M.-M., et al. 2007, Nature, 448, 1022

Jones, R.L., Gladman, B., Petit, J.-M., et al. 2006, Icarus, 185, 508

Kaib, N., Quinn, T. & Brasser, R. 2011, ApJ, 141, 3

Kaib, N., Roškar, R. & Quinn, T. 2011, Icarus, 215, 491

Kavelaars, J.J., Jones, R.L, Gladman, B., et al. 2009, AJ, 137, 491

Levison, H.F., Dones, L. & Duncan, M. 2001, AJ, 121, 2253

Levison, H., Morbidelli, A., Van Laerhoven, C., Gomes, R. & Tsiganis, K. 2008, Icarus, 196, 258

Luu, J., Marsden, B., Jewitt, D., et al. 1997, Nature, 387, 573

Minton, D., Richardson, J., Thomas, P., Kirchoff, M. & Schwamb, M. 2012, in ACM Conf. Sess 551

Morbidelli, A., Bottke, W.F., Nesvorný, D. & Levison, H. 2009, Icarus, 204, 448

Morbidelli, A., Emel'yanenko, V. & Levison, H.F. 2004, MNRAS, 355, 935

O'Brien, D. & Greenberg, R. 2005, Icarus, 178, 179

Petit, J.-M, Kavelaars, J.J., Gladman, B., et al. 2011, AJ, 142, 131

Sheppard, S. & Trujillo, C. 2006, Science, 313, 511

Sheppard, S. & Trujillo, C. 2010, ApJ, 723, L233

Solontoi, M., Ivezić, Ž., Jurić, M. et al. 2012, Icarus, 218, 571

Volk, K. & Malhotra, R. 2008, ApJ, 687, 714

Trujillo, C., Jewitt, D., & Luu, J. 2000, ApJ, 529, 103

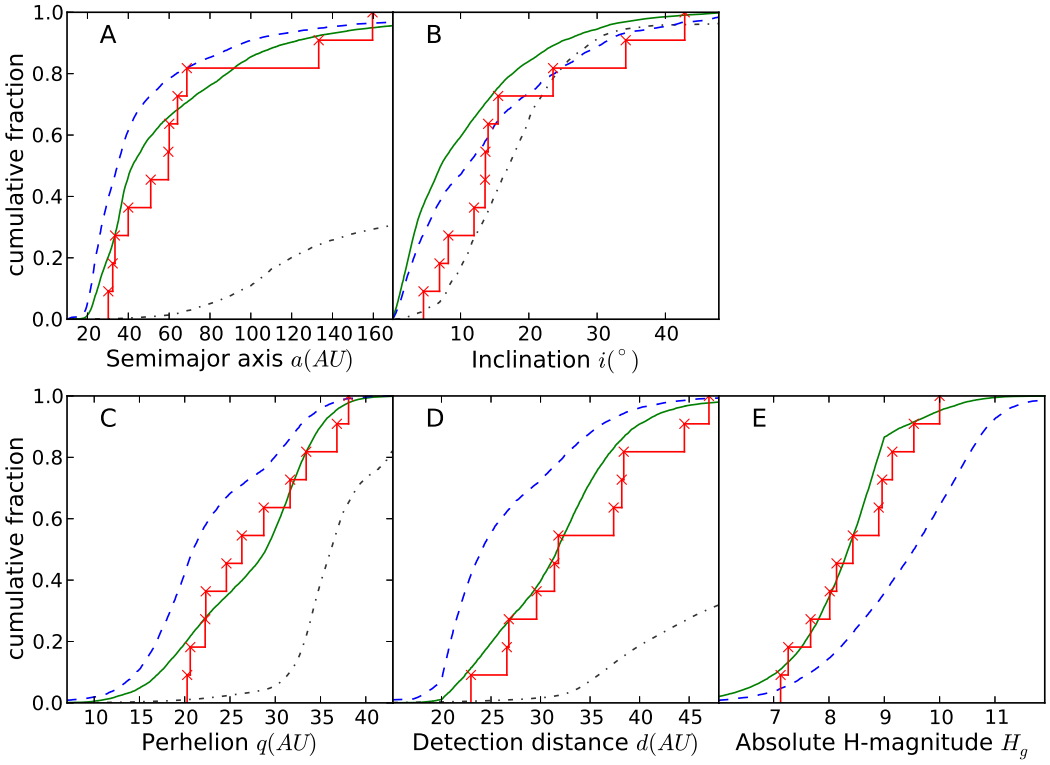

Fig. 1.— Cumulative distributions for 5 quantities, comparing the observed objects with the initially cold model's simulated detections. The black dash-dot curves show the orbital model's a, i, q, and d distributions; these differ from the detections (red staircase) due to observational biases. When coupled to two different $N(H_g)$ distributions, the biases produce the differing predictions for the detections. A single power-law slope of $\alpha = 0.8$ (blue dashed) is rejectable at $> 99\%$ confidence in d, q and H_g. Contrastingly, our preferred divot $N(H_g)$ (green curve, see Fig. 2) provides vastly better matches, although both produce too many low-i detections.

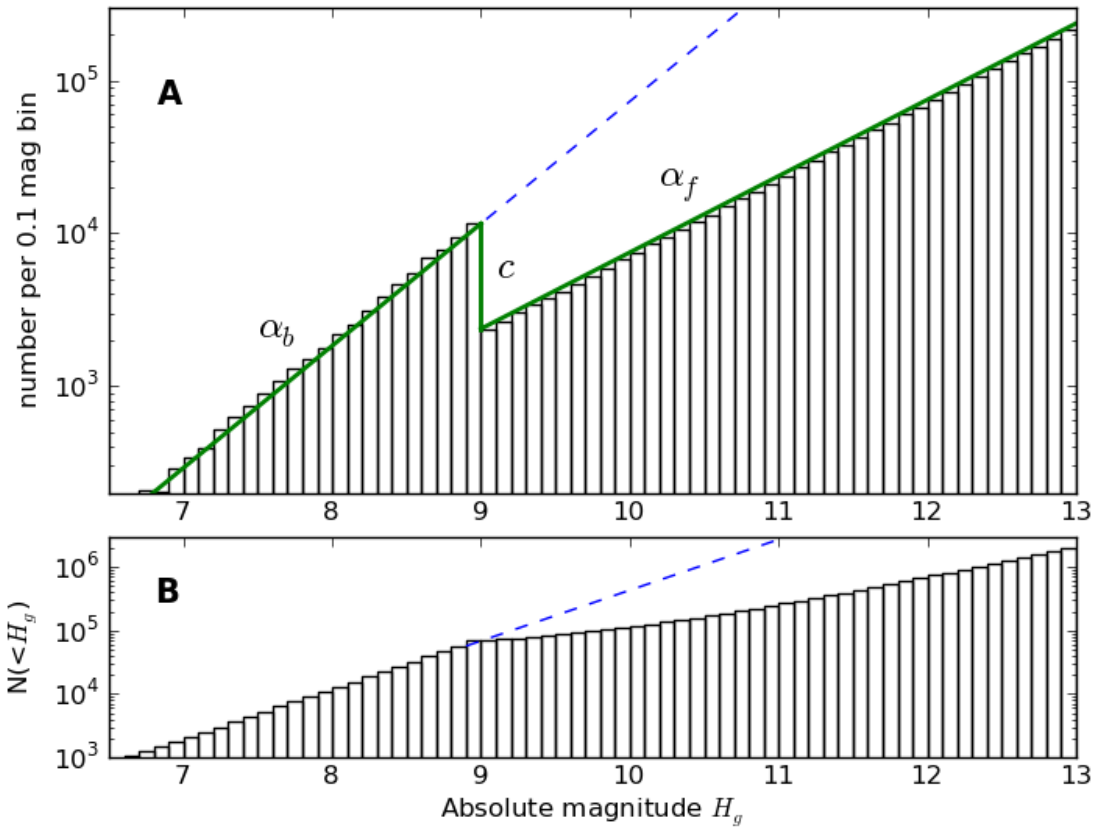

Fig. 2.— Histograms of the $N(H_g)$ distribution for our preferred divot solution. The vertical axes show the total SO numbers using the absolute CFEPS calibration (Petit et al. 2011). **A:** The differential distribution (solid green), with an extrapolated $\alpha = 0.8$ beyond $H_g = 9$ (dashed blue). The contrast $c \simeq 6$ is the ratio of differential number on either side of the divot. **B:** The cumulative version. For H_g >13 the cumulative $N(< H_g)$ has reached slope α_f after the flattened region beyond the divot.

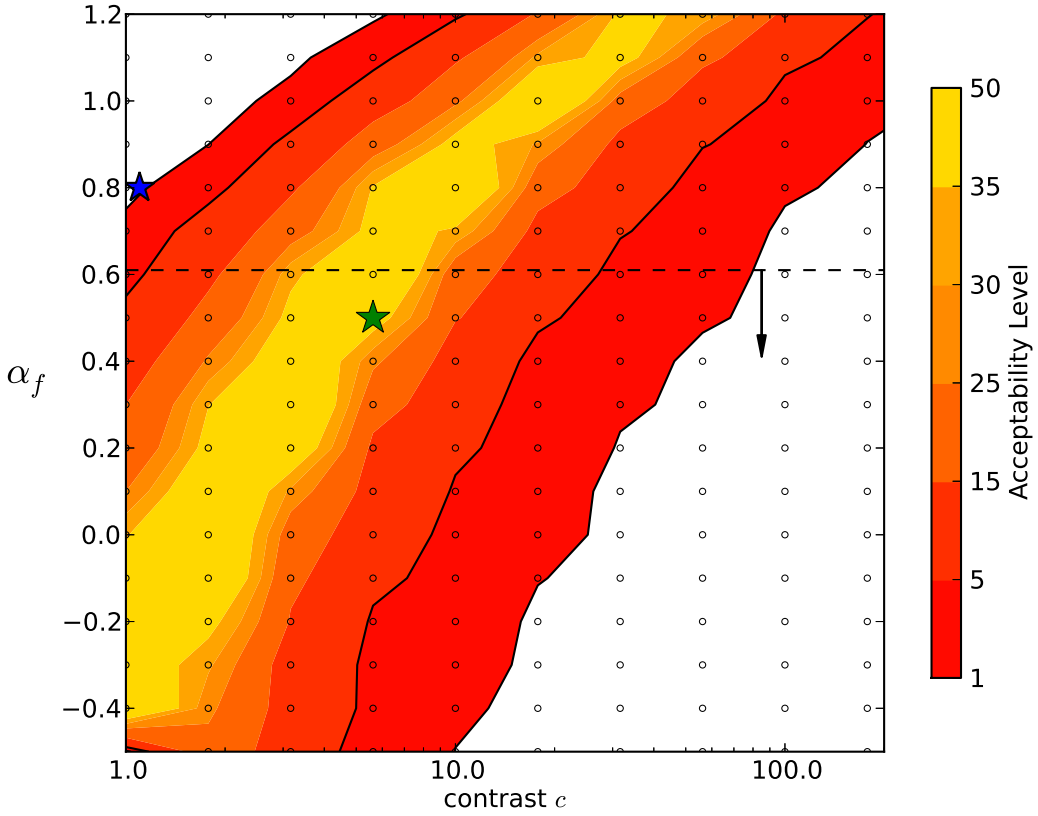

Fig. 3.— Contour values (colors) computed from a grid (points) in (c, α_f) space, giving the Anderson-Darling probability of drawing the most rejectable of the d, q, i, and H_g distributions from the model of today's scattering objects, from a hot initial population (see text). White areas indicate when the worst distribution had <1% probability of coming from the model, and the black contour bounds <5%. A single power-law (blue star) is rejected. Our favoured model (green star) satisfies both (a) $\alpha_f \simeq 0.5$ like known JFCs, (b) $\alpha \leq 0.6$ which prevents the extrapolated mass of small SOs from diverging.

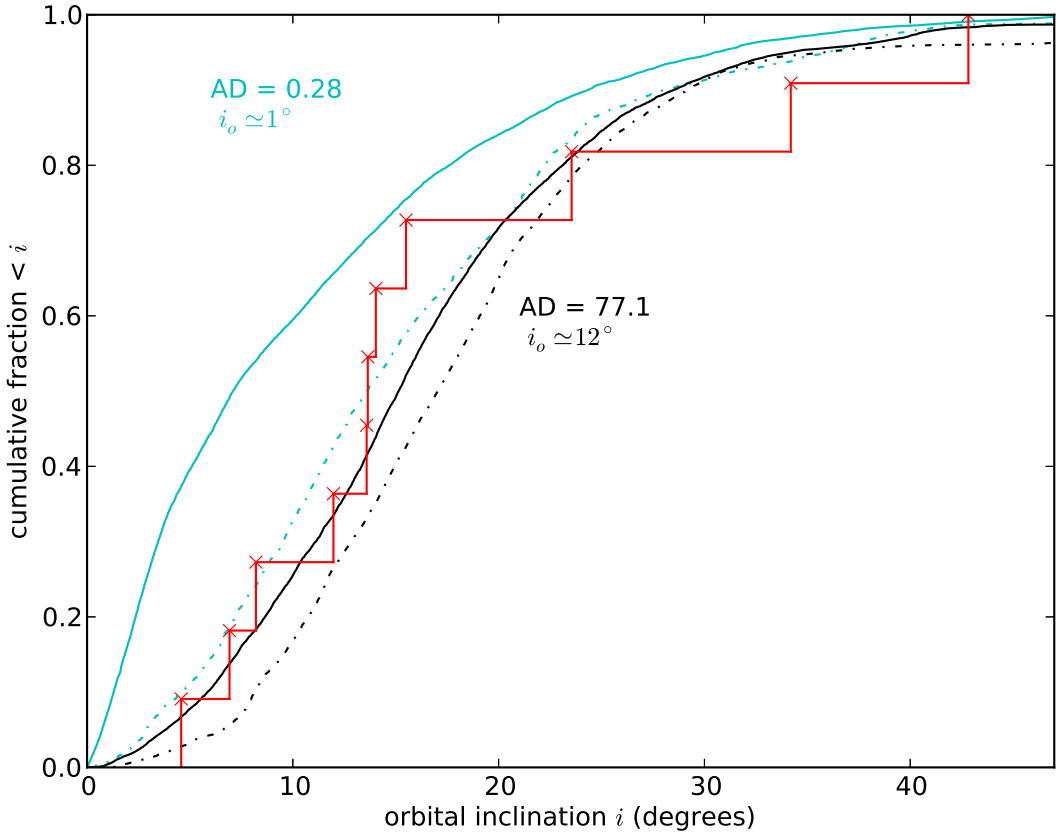

Fig. 4.— The hot (black dashed) and cold (light blue dashed) KRQ11 intrinsic i distributions produce the biased distributions (solid lines) for our preferred model for comparison with the CFEPS sample (red). The hot model significantly improves the match because it has a relative lack (at the current epoch) of low-i SOs to be detected by the survey; the eleven CFEPS SOs have $< 1\%$ probability of being drawn from the initially cold simulation because it predicts $i < 7^\circ$ survey detections should form about half the detected sample (solid light blue curve).

Designation	**a (AU)**	**e**	**i (deg)**	**d (AU)**	**H_g**
L4k09	30.19	0.18517	13.586	26.63	9.5
HL8a1	32.38	0.37406	42.827	44.52	7.3
L4m01	33.48	0.33308	8.205	31.36	8.9
L4p07	39.95	0.28088	23.545	29.59	7.7
L3q01	50.99	0.484	6.922	38.17	8.1
L7a03	59.61	0.43949	4.575	46.99	7.1
L4v11	60.04	0.62928	11.972	26.76	10.0
L4v04	64.10	0.50638	13.642	31.85	9.1
L4v15	68.68	0.6999	14.033	22.95	9.0
L3h08	159.6	0.7613	15.499	38.45	8.0
HL7j2	133.25	0.72374	34.195	37.38	8.4

Table 1: CFEPS actively scattering sample